Supporting information

A Superior δ-MnO$_2$ Cathode and a Self-Healing Zn-δ-MnO$_2$ Battery

Donghong Wang,[†] Lufeng Wang,[‡] Guojin Liang,[†] Hongfei Li,[†] Zhuoxin Liu,[†] Zijie Tang,[†] Jianbo Liang,[, ‡] Chunyi Zhi[*, †, §]*

[†] Department of Materials Science and Engineering, City University of Hong Kong, 83 Tat Chee Avenue, Kowloon, Hong Kong 999077, China

[‡] Department of Chemistry, Capital Normal University, 105 West Third Ring Road North, Haidian District, Beijing 100048, PR China.

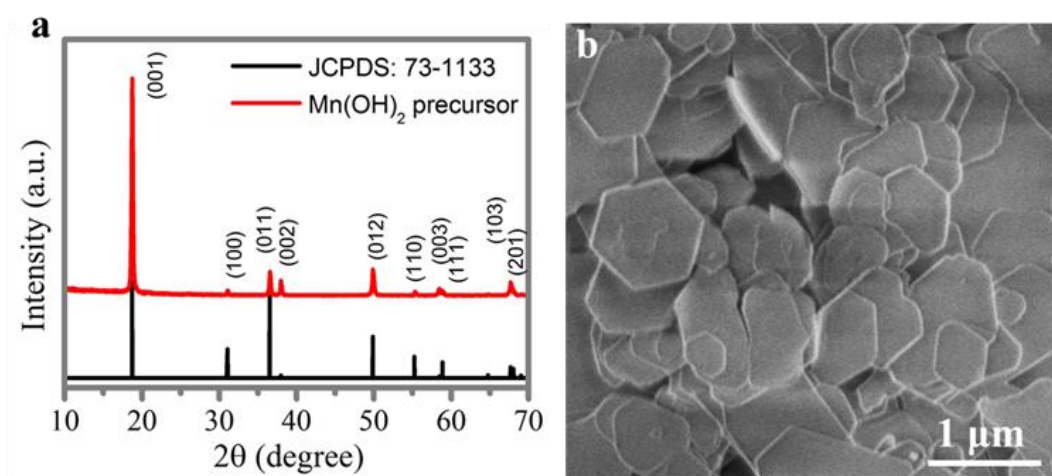[§] Shenzhen Research Institute, City University of Hong Kong, Shenzhen, PR China
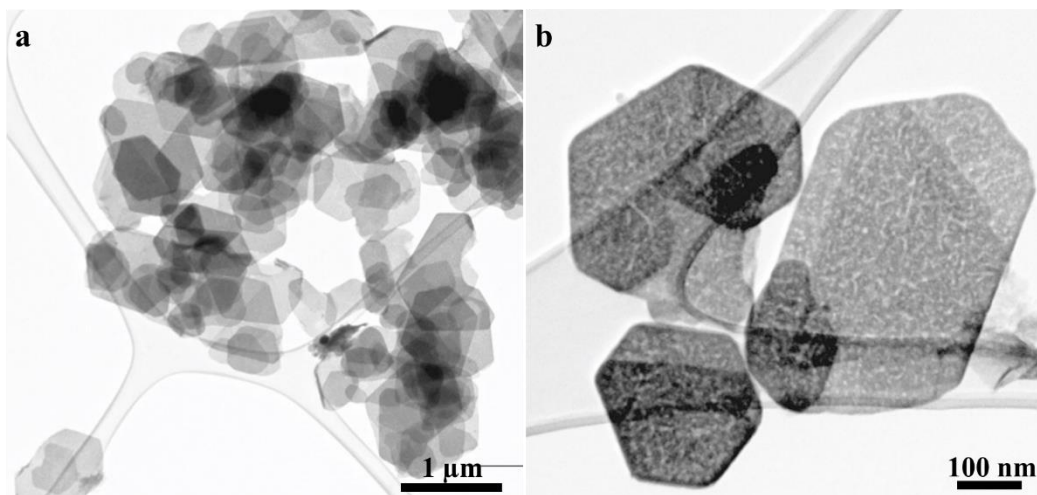
Figure S1. XRD and SEM of Mn(OH)$_2$ precursors.
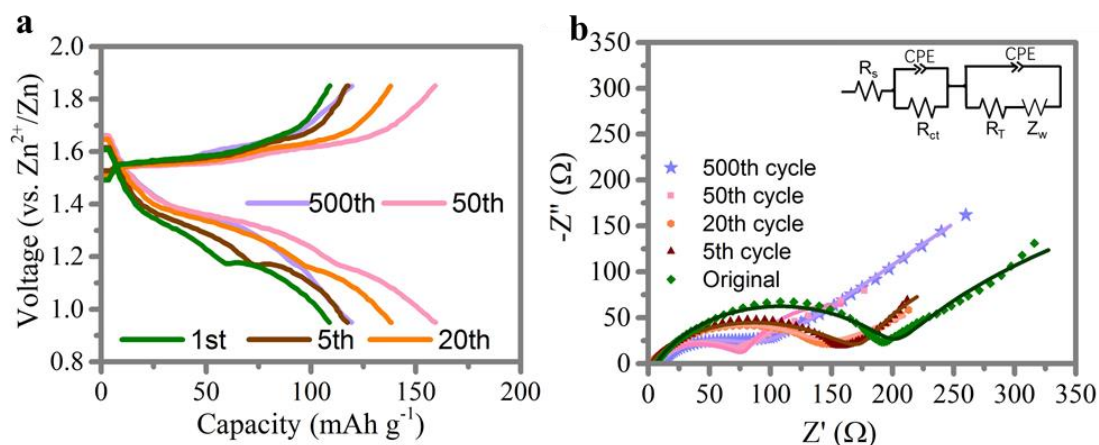
Figure S2. TEM images of δ-NMOH sample.

Figure S3. Activation process of Zn-δ-NMOH at 20 C: (a) Discharge-charge profiles

for selected cycles. (c) EIS curves measured at selected cycling cycles.

As shown in Figure 2f, the capacity gradually increases to the largest value at the

50th cycle, the corresponding discharge-charge profiles are shown in Figure S3, after

activation, the battery delivers a highest discharge capacity of 159 mAh g^{-1} at the 50th

cycle, and then decreases slightly and achieves an equilibrium around 110 mAh g^{-1}

since the 500th cycles (Figure 2f). The main cause was also studied *via* EIS

measurement, as shown in Figure S 3b, the results indicate that the charge transfer

impedance (Rct) decreases obviously at the 50th cycle, only half of the original one, after that the Rct bounces back slightly. The change perhaps is the dominant reason for the electrochemical activation.[1]
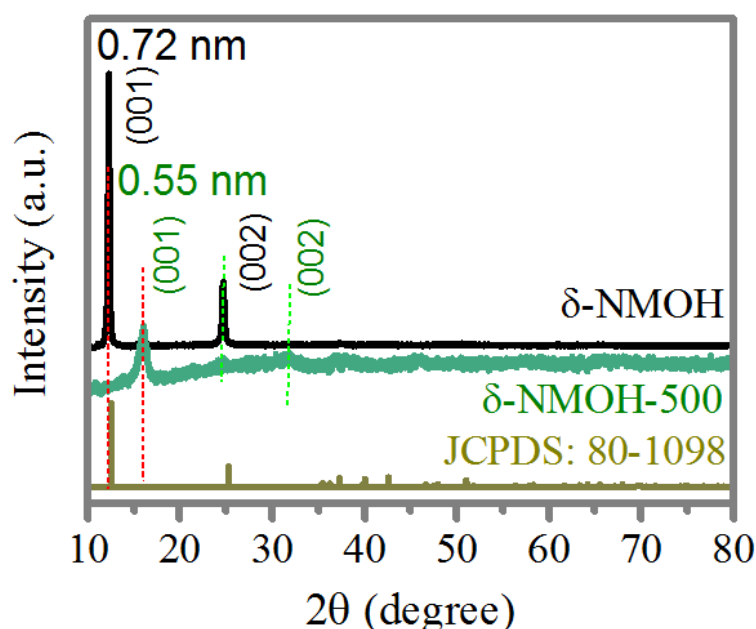

Figure S4. XRD patterns of δ-NMOH and δ-NMOH-500.

δ-NMOH-500 sample was obtained through a calcination process from room temperature to 500 °C with a heat rate of 10 °C/min, and the sample was kept at 500 °C for 5 mins. As shown in Figure S4, after the thermal treatment, the layered structure remained while the crystallinity decreased significantly. Furthermore, the interspace of (001) plane decreases from 0.72 nm to 0. 55 nm. Obviously, the removal of intercalated water molecules leads the shrinkage of the interlayer. In addition, the loss of water molecules decreases the steadiness of layered structure.
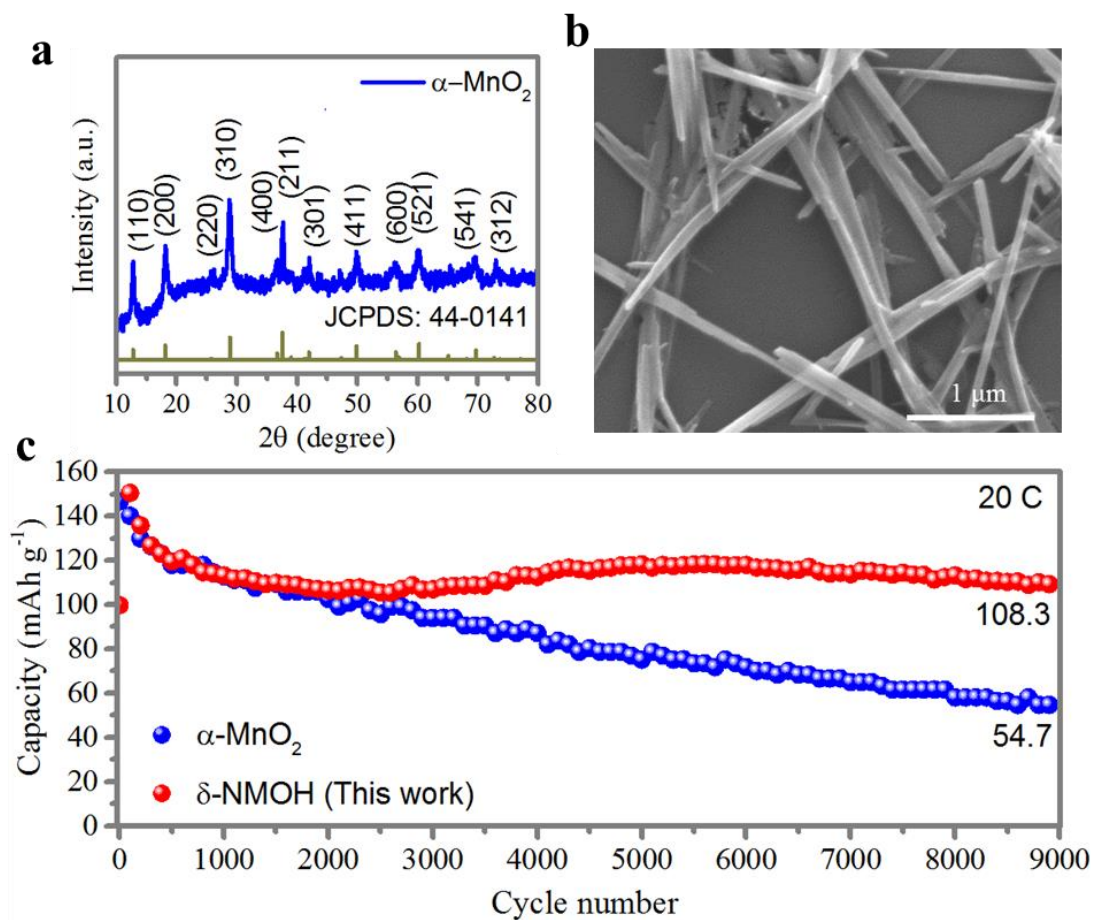
Figure S5. (a) and (b) SEM and XRD patterns of α-MnO₂, (c) comparison of cycling performance of α-MnO₂ and δ-NMOH.

As shown in Figure S5a and b, the as-prepared α-MnO₂ possesses a morphology of nanotubes. As a control, α-MnO₂ cathode delivers a much poorer cycling stability than δ-NMOH, with a discharge capacity of only 54.6 mAh g^{-1} remained after 9000 cycles at 20 C.
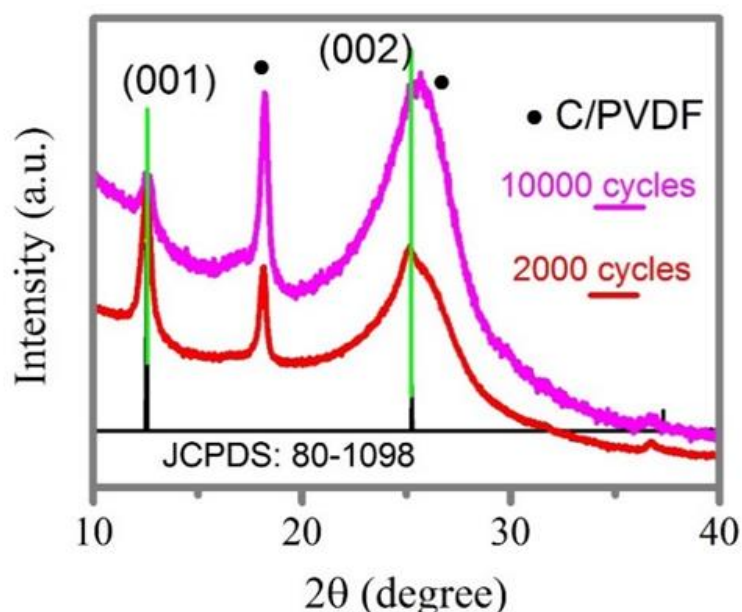
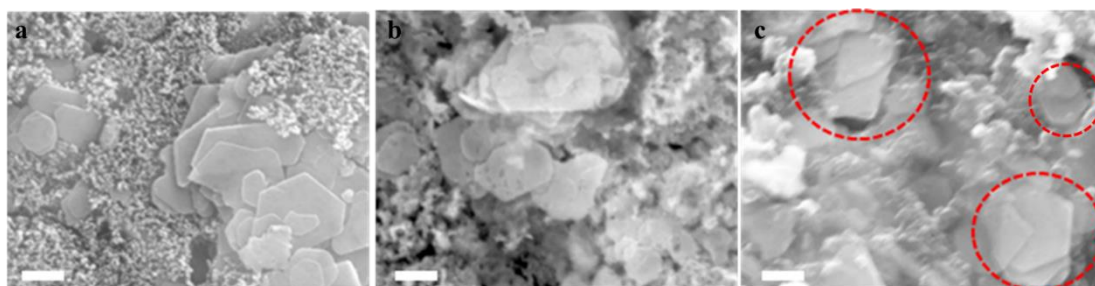Figure S6. XRD of the δ-NMOH cathode after cycled for 2000 cycles and 10000 cycles at 20 C.

Figure S7. SEM of δ-NMOH cathode at different stages: (a) pristine electrode, (b) after discharged to 0.95 V, (c) after charged to 1.85 V. (scale bars: 400 nm)

As shown in Figure S7b, a small portion of holes formed on the nanoplates as parts of the discharged products dissolved in electrolyte (Mn^{3+} formed during discharging tends to generate Mn^{4+} and Mn^{2+} through a disproportional reaction, while Mn^{2+} is soluble in electrolyte). However, the nanoplates recover after charge with an electrodeposition process of MnO_2. During the whole process, the shape of nanoplate

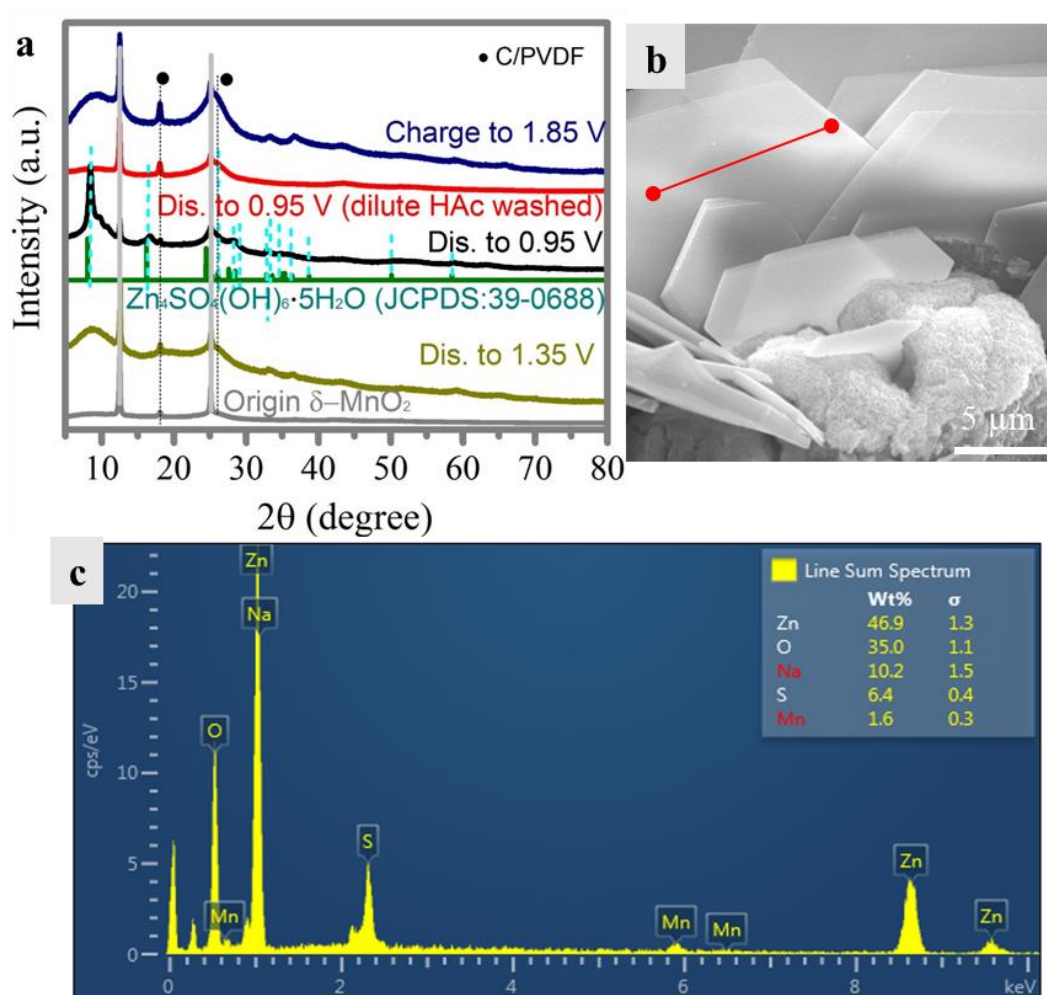preserves, this directly reflects the high stability of the δ-NMOH as the cathode for Zn ion battery.

Figure S8. (a) The ex-situ XRD patterns of δ-NMOH electrode. (b) SEM and the corresponding EDS spectra of the cathode discharged to 0.95 V.

For the only water-washed cathodes, when the cell was further discharged to 0.95 V, a series of different peaks appeared, which can be well indexed to $Zn_4SO_4(OH)_6 \cdot 4H_2O$ [2-4] (JCPDS: 39-0688) as shown in Figure S8a. The peaks assigned to

$Zn_4SO_4(OH)_6\cdot 4H_2O$ disappeared after charged to 1.85 V, and the cathode recovered back to its pristine structure. The presence of $Zn_4SO_4(OH)_6\cdot 4H_2O$ also can be detected through SEM and EDX, as exhibited in Figure S8b, large nanosheets were scanned on the surface of the cathode, and the composition was confirmed through EDS measurement (Figure S5c), a large amount of Zn and S were detected with a molar ratio of 3.6. After removed the $Zn_4SO_4(OH)_6\cdot 4H_2O$ with dilute acetic acid,[3] layered structure of MnO_2 presented as the product discharged to 0.95 V (Figure S8a).
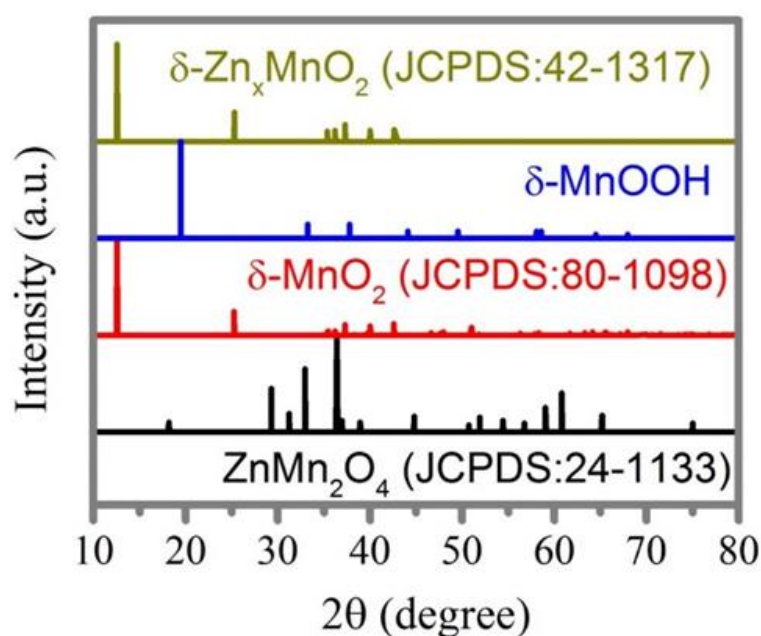

Figure S9. Standard XRD patterns of layered Zn_xMnO_2, layered MnOOH, layered MnO_2 and $ZnMn_2O_4$ for comparison
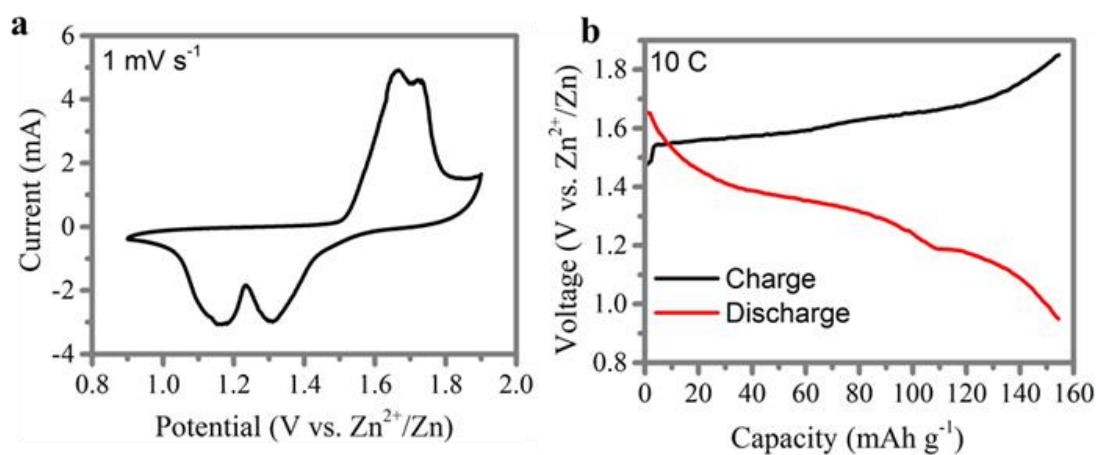
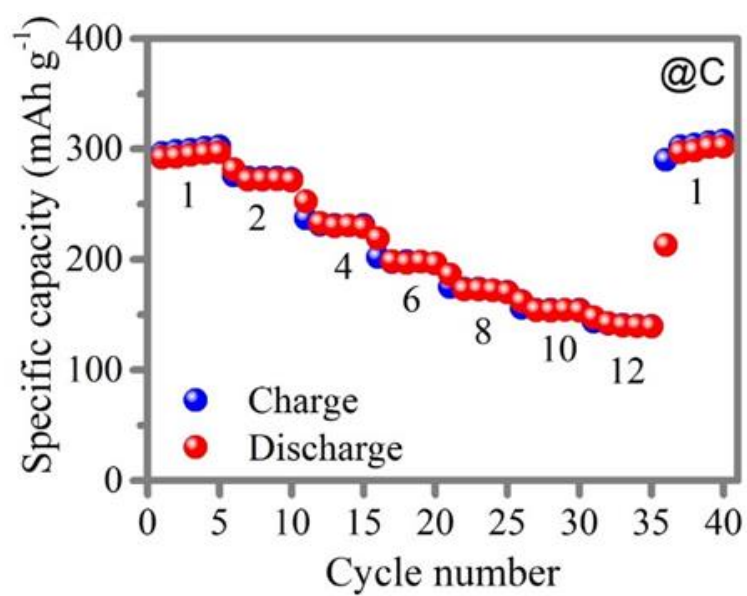Figure S10. CV curve (a) and discharge-charge curve (b) of Zn-δ-NMOH battery in

PAM hydrogel.

Figure S11. Cycling performance at various C-rates (1 C-12 C) for Zn-δ-NMOH battery
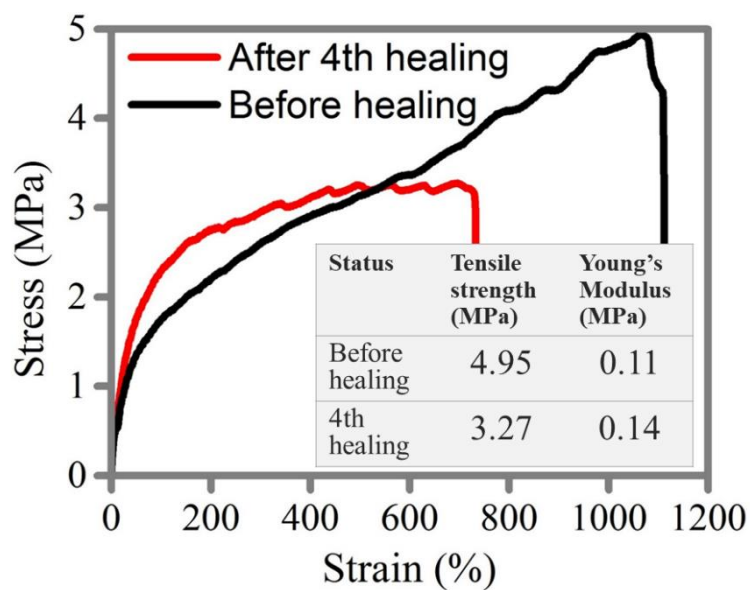
in PAM.

Figure S12. Tensile measurements of the pure CPU before the cut, after 4 times cut/healing, with the inset table showing the corresponding tensile strength and Young's Modulus.
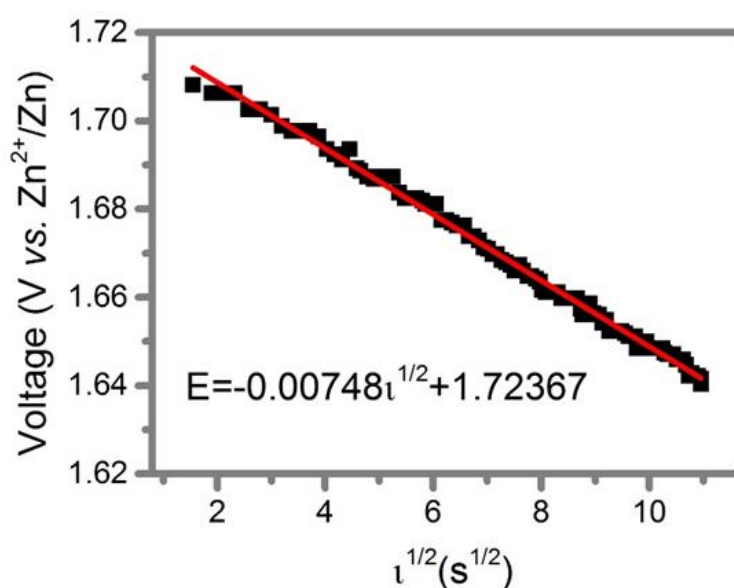

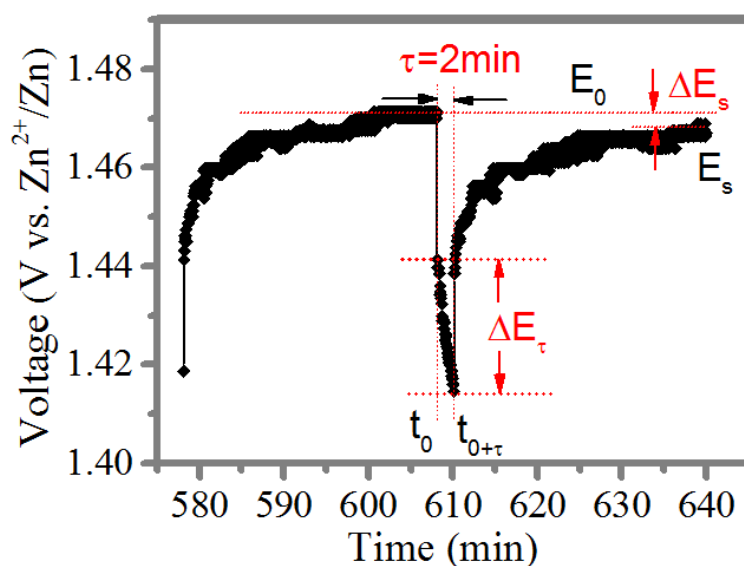Figure S13. Linear behavior of the E vs $\tau^{1/2}$ relationship

Figure S14. E *vs* t profile of δ-NMOH for a single GITT titration.

REFERENCES

1. Hao, J.; Mou, J.; Zhang, J.; Dong, L.; Liu, W.; Xu, C.; Kang, F., Electrochemically Induced Spinel-Layered Phase Transition of Mn_3O_4 in High Performance Neutral Aqueous Rechargeable Zinc Battery. *Electrochim. Acta* **2018,** *259*, 170–178.

2. Huang, J.; Wang, Z.; Hou, M.; Dong, X.; Liu, Y.; Wang, Y.; Xia, Y., Polyaniline-Intercalated Manganese Dioxide Nanolayers as a High-Performance Cathode Material for an Aqueous Zinc-Ion Battery. *Nat. Commun.* **2018,** *9*, 2906.

3. Lee, B.; Seo, H. R.; Lee, H. R.; Yoon, C. S.; Kim, J. H.; Chung, K. Y.; Cho, B. W.; Oh, S. H., Critical Role of pH Evolution of Electrolyte in the Reaction Mechanism for Rechargeable Zinc Batteries. *ChemSusChem* **2016,** *9*, 2948–2956.

4. Kim, S. H.; Oh, S. M., Degradation Mechanism of Layered MnO_2 Cathodes in Zn/$ZnSO_4$/MnO_2 Recharagable Cells. *J. Power Sources* **1998,** *72*, 150–158.